

Research paper

Dielectric properties of diamond using an X-band microwave split dielectric resonator

Jerome A. Cuenca^{a,*}, Soumen Mandal^a, Jaspa Stritt^a, Xiang Zheng^b, James Pomeroy^b, Martin Kuball^b, Adrian Porch^c, Oliver A. Williams^a

^a School of Physics and Astronomy, Cardiff University, Cardiff, CF24 3AA, United Kingdom

^b Center for Device Thermography and Reliability, University of Bristol, Bristol, BS8 1TL, United Kingdom

^c School of Engineering, Cardiff University, Cardiff, CF24 3AA, United Kingdom

ARTICLE INFO

Keywords:

Diamond
Microwave
Dielectric resonator
Complex permittivity
Chemical vapour deposition
X-band

ABSTRACT

This work presents an easy-to-use microwave split dielectric resonator (MSDR) for X-band dielectric measurements of free-standing unpolished poly-crystalline diamond (PCD). PCD grown with varying CH₄/H₂ and O₂/CH₄/H₂ in the gas phase show stark differences in dielectric loss. Low microwave dielectric loss PCD is found for CH₄/H₂ concentrations of less than 5% while PCD grown with O₂ show very high loss tangents. Vacuum annealing introduces non-diamond carbon (NDC) impurities which increases the loss, however, even after significant discolouration the loss is still lower than the O₂ grown PCD. The loss mechanism of O₂ grown PCD is likely due to a high concentration of grain boundaries and grain boundary hopping conduction mechanisms as opposed to high concentrations of NDC impurities.

1. Introduction

Free-standing chemical vapour deposited (CVD) diamond is a valuable high thermal conductivity dielectric for high power electronics [1] and also has a number of low complex permittivity ($\epsilon_r^* = \epsilon_r' - j\epsilon_r''$) microwave X-band (8–12 GHz) applications, including microwave resistors [2,3] and high electron mobility transistors [4]. While there are several studies on the microwave dielectric properties of free-standing diamond, these are typically at very high frequencies (>100 GHz) which use Fabry Perot techniques [5–8] or THz waveguide systems [9]. For X-Band, evaluation of ϵ_r^* and the loss tangent ($\tan \delta_e = \epsilon_r''/\epsilon_r'$) involves microwave broadband transmission/reflection methods or resonator approaches [10–14]. The most direct method is to fabricate a coplanar transmission line on the substrate, but this requires a lithography step onto the diamond substrates [14].

To circumvent lithography, non-contacting X-band waveguide and cavity resonator methods can be used. Large and specific sample areas are typically needed to perfectly occupy the cavity and avoid depolarisation fields; for example, a standard WR112 X-Band cross-sectional area is 28.5 × 12.6 mm. Geometrical constraints can be eased using perturbation methods such as the system presented by Molla et al. while Parshin et al. have shown a cylindrical cavity resonator system

for diamond discs, reporting $\tan \delta_e$ values lower than $\sim 10^{-4}$ [10,15,16]. However, in both air-spaced waveguide and cavity approaches, the sample dimensions must still be machined to fit flush within the cavity walls. It is also possible to fabricate an entire resonator out of the diamond, where Floch et al. show samples with $\tan \delta_e$ values of $\sim 10^{-3}$ [17]. For X band characterisation of wholly diamond resonators then the size becomes unfeasibly large at great cost (cm dimensions). However, sample miniaturisation is possible using the microwave split dielectric resonator (MSDR) method as is presented by Krupka et al. for various ceramics [18,19].

This work presents an MSDR system for the quality control of diamond plates, designed for ease of use using a split cavity with two high dielectric constant, low loss ceramics to focus the electromagnetic (EM) fields into a small volume, reducing the sample size requirements for X-Band diamond measurements ($\sim 10 \times 10 \times 0.5$ mm). Using a magnetic clasp cavity design, fast quality control measurements can be achieved at a nominal resonant frequency of 8.3 GHz with access to a higher order K-band mode at 16.1 GHz. Dielectric measurements are presented of free-standing CVD diamond plates deposited using various microwave plasma chemical vapour deposition (MP-CVD) recipes.

* Corresponding author.

E-mail address: cuencaj@cardiff.ac.uk (J.A. Cuenca).

<https://doi.org/10.1016/j.carbon.2024.118860>

Received 30 November 2023; Received in revised form 24 January 2024; Accepted 24 January 2024

Available online 25 January 2024

0008-6223/© 2024 The Author(s). Published by Elsevier Ltd. This is an open access article under the CC BY license (<http://creativecommons.org/licenses/by/4.0/>).

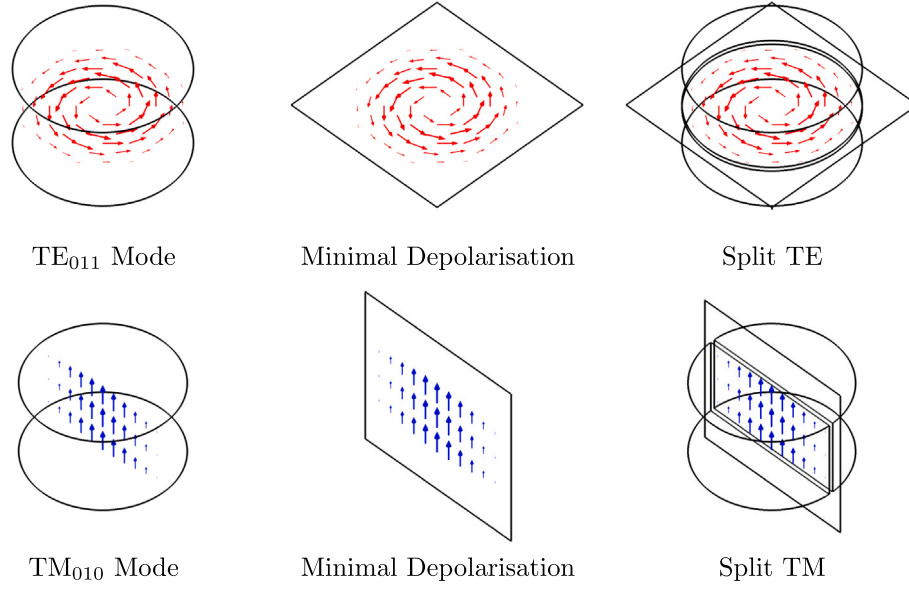


Fig. 1. Schematic of non-depolarisation field requirements for MSDR, with arrows showing E-field vectors for the cylindrical TE₀₁₁ and TM₀₁₀ configurations.

2. Model

2.1. Theoretical model

Microwave cavity perturbation (MCP) is a well-known method for permittivity measurements of carbonaceous materials, including diamond [20–23]. The change in frequency (f) and -3 dB quality factor (Q) of a microwave resonator from the unperturbed state to the sample perturbed state can be used to extract the complex permittivity and permeability. For non-magnetic plate samples, permittivity measurements are typically extracted in minimal depolarisation field configurations for high sensitivity, shown in Fig. 1 for cylindrical transverse electric (TE) and magnetic (TM) resonators. In the minimal depolarisation configuration, complex permittivity can be extracted using the following MCP approximation [22,24]:

$$\epsilon'_r \approx 2 \frac{f_0 - f_s}{f_0} \frac{V_m}{V_s} + 1 \quad (1)$$

$$\epsilon''_r \approx \left(\frac{1}{Q_s} - \frac{1}{Q_0} \right) \frac{V_m}{V_s} \quad (2)$$

where f is the resonant frequency of the cavity, Q is the quality factor, ‘0’ and ‘s’ denote the unperturbed and sample states, $V_m = G_m t$ is the mode volume, G_m is a linear calibration constant and V_s and t are the sample volume and thickness, respectively. For ease of construction, split cylindrical TE modes can be formed by stacking 2 resonators. The resonant frequency of the system can be designed and estimated to operate in the X-band using the theoretical solution for an ideal dielectric cylinder surrounded by perfect electrical conductors (PEC):

$$f_0 = \frac{c}{2\pi \sqrt{\epsilon_{r,c} \mu_{r,c}}} \sqrt{\left(\frac{\alpha'_{mn}}{a} \right)^2 + \left(\frac{p\pi}{l} \right)^2} \quad (3)$$

where c is the speed of light in free space, $\epsilon_{r,c}$ and $\mu_{r,c}$ are the permittivity and permeability of the cavity, respectively and α'_{mn} is the n th root of the $J'_m(x)$ Bessel function, as appropriate for the E field boundary conditions for TE modes, a and l are the cavity radius and height, respectively, m, n are integers and p is the longitudinal integer mode number.

Diamond samples are typically low loss and small in size ($\sim 10 \times 10 \times 0.5$ mm) and so placing a diamond inside of a larger cavity resonator will result in a small change in f and Q . To increase the sensitivity, either larger diamonds can be made (increase V_s) or the cavity can be made smaller such that the E-field is focused into

a smaller volume (decrease V_m or G_m). For the latter, maintaining X-band operation whilst miniaturising can be achieved by increasing $\epsilon_{r,c}$. This becomes a very useful alternative to waveguide methods which require large samples. With EM fields focused, the central regions of diamond plates can be probed with minimal sensitivity to the edges and reduce any depolarisation effects, making the measurement highly reproducible. The only sample requirement is a known thickness. Practically, stacked TE resonators are better suited over TM modes for plate samples as is shown in Fig. 1, where this work uses the circulating TE₀₁₁ and TE₀₁₃ modes. For 10×10 mm CVD diamond substrates, restrictions on the DR radius ($a < 5$ mm) and the aspect ratio ($l < 2r$) are needed to fulfil non-depolarisation and reduce interference from unwanted higher TM modes.

Fig. 2a and b show the theoretical resonant frequency for the TE₀₁₁ mode as a function of $\epsilon_{r,c}$ and feasible resonator dimensions. As shown in Fig. 2a although shorter heights offer the least TM interference, a very high $\epsilon_{r,c}$ is needed for X-band operation. The proposed MSDR design (denoted ‘DR’ in Fig. 2b) uses a total height of 4 mm (or 2× stacked 2 mm resonators separated by a 0.5 mm gap) which can be easily achieved using commercial dielectrics; 2× stacked T-Ceram E-37 dielectrics, $a = 3.5$ mm and $l/2 = 2$ mm.

2.2. Numerical model - Practical design

Modifications such as coupling antennas, sample slots and housing introduce discontinuities in the field distribution and alter the resonant frequency which cannot be estimated using Eq. (3). Their effects on the resonance can be investigated using finite element modelling (FEM), with discretisation of a 3D geometry into domains/nodes and solving for both eigenfrequency and frequency domain solutions of Maxwell’s equations. FEM also ensures that modes can be identified through both their eigenvalues and simulated S parameters in the frequency domain to ensure the correct mode is identified in practice, as shown in later sections.

Fig. 3 shows the E-Field of the TE₀₁₁ mode (also known as the TE_{01δ} mode for dielectric resonators, but henceforth referred to simply as the TE₀₁₁ mode) and the calculated eigenfrequency with incremental modifications. An ideal cylindrical dielectric resonator encased in PEC has a nominal frequency of 10.6 GHz (Fig. 3a). Introducing an air-spaced gap allows the E-field to spill into sample measuring space which marginally increases the frequency to 11.7 GHz (Fig. 3b). Since

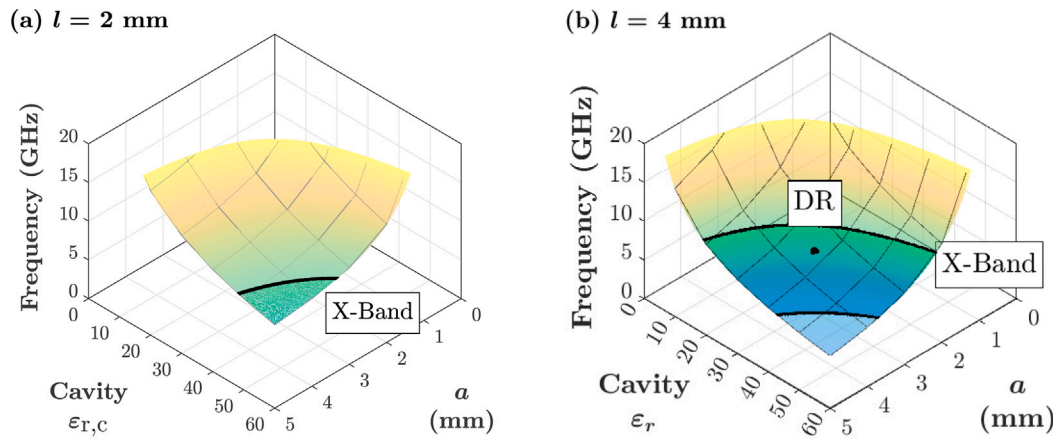


Fig. 2. Theoretical frequency design requirements for the TE_{011} mode where a and l denote the cylindrical radius and length, respectively and $\epsilon_{r,c}$ is the dielectric constant of the cylinder. The darker region denotes the X-band frequency range (8 to 12 GHz) and the point ‘DR’ denotes the chosen design.

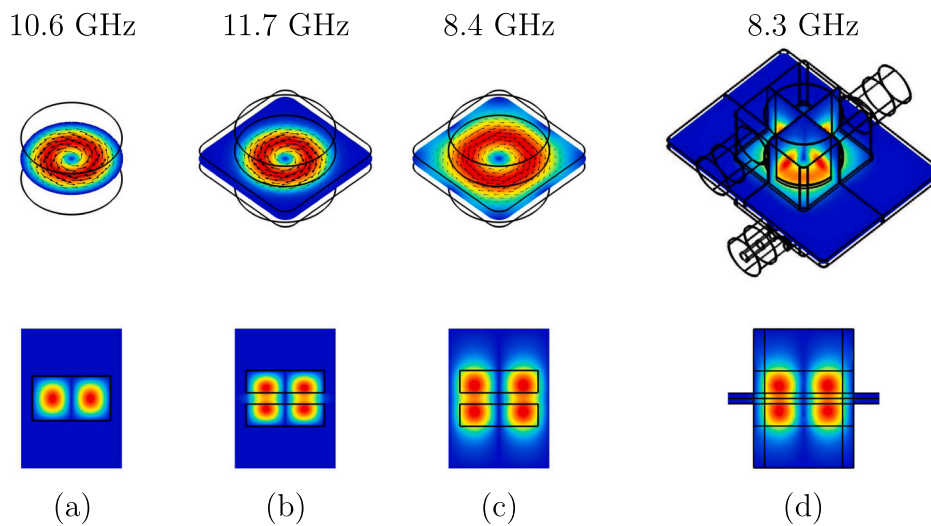


Fig. 3. FEM normalised E-field distributions of a cylindrical resonator ($a = 3.5$ mm and $l = 4$ mm). All outer extremities are modelled as PEC boundaries. Models show (a) air cavity $\epsilon_{r,c} = 1$ and dielectric resonator $\epsilon_{r,c} = 37$ at $f_0 = 64.3$ and 10.6 GHz, respectively (b) a split dielectric with a 1 mm air gap at $f_0 \approx 11.7$ GHz (c) a split dielectric housed in a PTFE support at $f_0 \approx 8.4$ GHz and (d) a split dielectric in PTFE with hull housing including coupling antennas and sample slot $f_0 \approx 8.3$ GHz.

DR ceramics are fairly brittle, a malleable and low permittivity polytetrafluoroethylene (PTFE) support is used to maintain the gap height as opposed to a metal cavity (Fig. 3c). This modification results in a frequency reduction to 8.4 GHz and E-field spillage into the PTFE although remains circulating within the sample region. Finally, the coupling structures, housing and a recess to support $20 \times 15 \times 1$ mm plates results in a small frequency reduction to 8.3 GHz (Fig. 3d). It is also important to note that the cross section in Fig. 3d shows that the active E-field region is contained to 9×9 mm area, with the highest sensitivity in the 7 mm diameter region in-between the dielectrics.

3. Method

3.1. Microwave measurements

An exploded schematic of the MSDR is shown in Fig. 4. The housing is made of 2 pieces of aluminium which snap together using alignment posts and magnets. The pieces are made with point symmetry for ease of duplication during machining. A $15 \times 20 \times 0.5$ mm recess is machined into each half for a total sample gap of ~ 1 mm. PTFE inserts suspend $2 \times$ stacked T-Ceram E-37 dielectric resonators ($a = 3.5$ mm, total l height of 4 mm). Coaxial SMA antennas on the base of the structure provide

E-field coupling to the TE modes for S_{21} measurements using a Keysight N5232A vector network analyser (VNA).

The calibration constant ‘ G_m ’ was obtained using a quartz sample of known permittivity and thickness ($\epsilon_r = 3.8$, $t = 500$ μm). A PTFE sheet was also measured to corroborate the calibration ($\epsilon_r \approx 2.05$ to 2.1 , $t = 505$ μm). Sample measurements were conducted $N = 10$ times, to average uncertainty in sample positioning and differences in the positioning of the two halves of the cavity. The cavity positioning error is the main source of random error, however is minimised using the magnets and alignment posts. The gap height error is therefore less important, and only the sample thickness is the critical parameter.

Fig. 5 shows the S_{21} spectra obtained by FEM and measurement. Owing to the tolerance in the positioning of the DR’s in the PTFE, the simulated FEM results show a sample gap of 0.9 mm as opposed to 1 mm, thereby lining up with the experimental S_{21} data. The TE_{011} mode has an unperturbed frequency of 8.3 GHz and an unloaded Q factor of 3445, with random measurement errors of 0.5% and 0.1%, respectively. TE_{012} has a nominal frequency of 10.1 GHz and unloaded Q factor of 3768 with errors of 1.5% and 0.1%, respectively and TE_{013} has an unperturbed resonance frequency of 16.1 GHz and unloaded Q-factor of 2719, respectively with random errors of 0.1% and 0.1%. Since the spectrum is fairly crowded, FEM is very important for identifying the practical high Q factor modes as labelled and highlighted

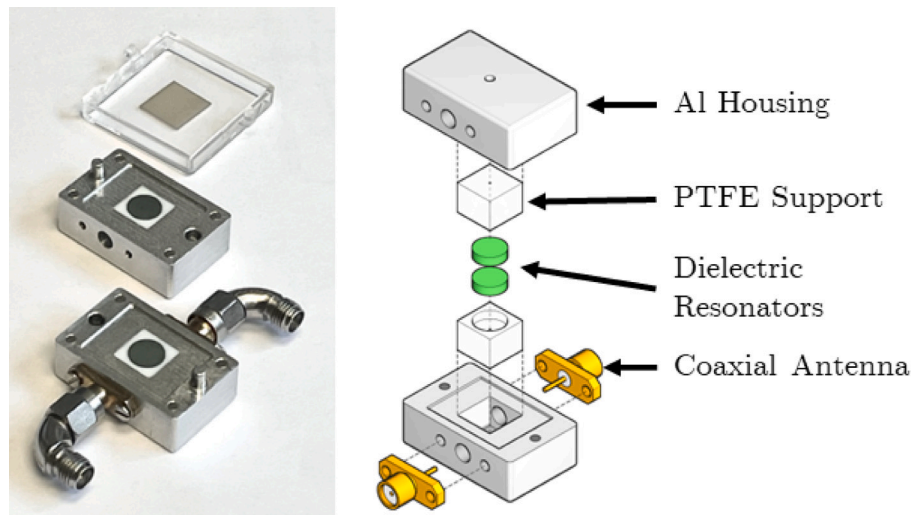


Fig. 4. Photograph of MSDR system with an $11 \times 11 \text{ mm}^2$ CVD diamond plate for size reference (left) and an exploded schematic (right).

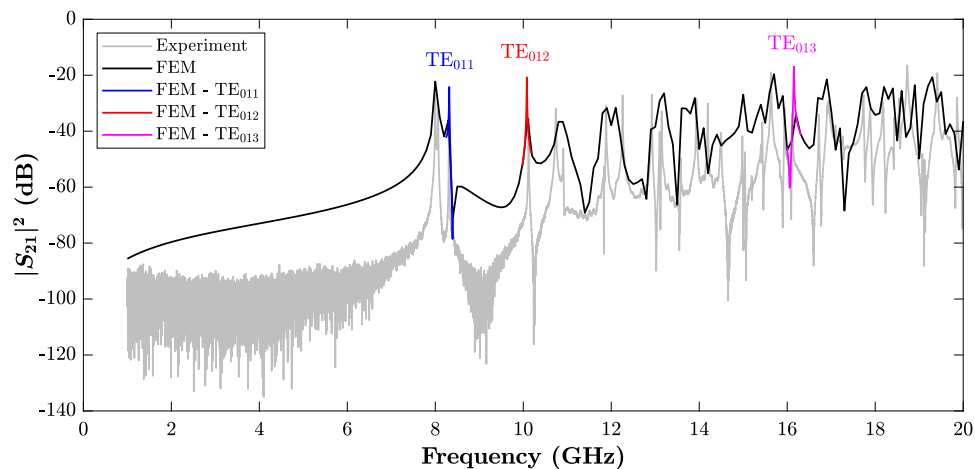


Fig. 5. Experimental and FEM wideband S_{21} transmission spectra. Mode 0, 1 and 2 denote the TE_{011} , TE_{012} and TE_{013} modes, respectively. FEM shows spectra for a sample gap of 0.9 mm.

in blue, red and magenta. The interference from other modes seems problematic at first, however, the majority of these modes shift when the sample is introduced. The sensitivity is moderately high for quick and easy bench-top measurements (<30 s). Loss tangent measurements are limited by the finite loss of the dielectrics themselves, imposing a systematic measurement limit of $\tan\delta_{\min} \sim 1.4 \times 10^{-3}$.

3.2. Diamond samples

Table 1 shows the various unpolished CVD diamond samples measured in the MSDR. Films were grown using MP-CVD with thicknesses of less than 0.2 mm and square areas larger than $10 \times 10 \text{ mm}^2$ to fully cover the 7 mm diameter dielectrics. The films were grown on Si using a standard nanodiamond seeding process [25,26], followed by exposure to a microwave CH_4/H_2 plasma at 5.5 kW at pressures > 140 mbar in gas flows > 300 sccm in a Carat Systems CTS6U using the small sample holder described in [27–30]. The samples were then laser diced using an Oxford Lasers A-Series Laser Micromachining System equipped with a pulsed 1064 nm Neodymium-doped yttrium orthovanadate (Nd:YVO4) solid state laser, frequency doubled to 532 nm (Innolas NANIO 521-10-V). The nominal power output was 11.4 W at 40 kHz, with a pulse width of <30 ns and a pulse-to-pulse stability of < 1% focused to a spot size of $\sim 3 \mu\text{m}$. The Si was then wet etched






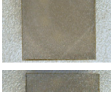
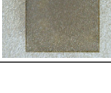
using a mixture of hydrofluoric acid, nitric acid and acetic acid [31] to produce free-standing unpolished diamond films.

In the first set, films were grown with a CH_4/H_2 concentration of 3 and 5%. The deposition duration was adjusted to accommodate variations in growth rate (24 and 18 h for 3% and 5%, respectively). The increased CH_4/H_2 concentration was used in an attempt to introduce more NDC impurities, and thus lower quality films [32–34]. In the second set, 0.2% O_2/H_2 was introduced to the gas phase for a fixed CH_4/H_2 concentration of 4%. O_2 is known to reduce the formation of NDC impurities but also reduce the growth rate [33]. To compensate for the increased etching, the growth was conservatively extended to 72 h. Finally for the third set, a film grown at 3% CH_4/H_2 was vacuum annealed in a furnace at 800°C at cumulative increments of 2, 7 and 15 h, to introduce very high concentrations of NDC impurities. With the exception of sample 3A, samples were successfully diced to areas greater than $10 \times 10 \text{ mm}$. 3A was damaged on silicon release and resulted in a smaller sample which still covers the 7 mm active DR diameter.

Qualitative measurements of non-diamond carbon (NDC) impurities were achieved with Raman spectroscopy using a Horiba LabRAM HR Evolution, equipped with 3 excitation lasers ($\lambda_e = 473, 532$ and 660 nm) and a $50\times$ objective. All spectra are obtained from the seeded side of the PCD film or the smaller grain side, as opposed to the growth or larger grain side in order to obtain sensitive characterisation of grain

Table 1

Summary of unpolished PCD samples used in this study. 3A-15 shows 3A after 15 h of vacuum annealing at 800 °C. 3A, 3B, 5A and 5B have been diced to 11 × 11 mm with some damage on 3A while 4AO and 4BO are diced to 10 × 10 mm.

ID	Image	CH ₄ (%)	O ₂ (%)	P _{in} (kW)	p (mbar)	Time (h)	t (μm)
3A		3	0	5.5	160	24	50
3A-15				15 h Vacc. anneal			
3B		3	0	5.5	160	24	54
5A		5	0	5.5	160	18	76
5B		5	0	5.5	160	18	68
4AO		4	0.2	5.5	147	72	116
4BO		4	0.2	5.5	147	72	122

boundary impurities. Scanning electron microscopy (SEM) images were obtained using a Thermo Scientific Phenom at an acceleration voltage of 5 kV.

4. Experimental results

4.1. Diamond recipe variation

Fig. 6a and b shows magnified MSDR VNA traces of the TE₀₁₁ and TE₀₁₃ modes, respectively, for the diamond plates grown with different recipes. All samples shift the unperturbed response to lower frequencies and reduce the Q factor, the overall magnitude of which also varies depending upon the dielectric properties and volume of the sample. For both TE₀₁₁ and TE₀₁₃, there are small differences in the complex frequency shift owing to the varying thicknesses. The calculated complex permittivity in Fig. 6c to f show small differences in dielectric constant and almost no measurable difference in loss between all of the samples grown at varying CH₄ concentrations with no O₂ in the gas phase. However, for samples grown with O₂ in the gas phase, a considerable damping of the Q factor is observed at both 8.3 GHz and 16.1 GHz. It is clearly shown that PCD grown using MP-CVD with O₂ in the gas phase significantly increases the microwave absorption.

Fig. 7a to c shows the Raman spectra of the diamond films grown with different CH₄/H₂ concentrations in addition to the samples with O₂ in the gas phase. The results for all wavelengths show a sharp peak at ~1332 cm⁻¹, associated with the first order sp³ bonded carbon peak, a characteristic signature of diamond. Fig. 7d and e show the Lorentzian peak position and full-width at half maximum (FWHM), respectively, which in general show that the sp³ carbon peak is shifted to towards higher wavenumbers, implying that the intrinsic film stress tends towards compression [35]. This is better observed at λ_e = 473 nm, however is less conclusive for λ_e = 532 nm and λ_e = 660 nm which show a randomly varying and overall lower peak position at ~1332 cm⁻¹. This is likely due to the fact that higher wavelength lasers are far more sensitive to resonance and scattering caused by sp² carbon and NDC impurities owing to the greater cross-section compared to sp³ carbon [36]. Excitation wavelengths towards UV are therefore better

suitable for examining the diamond crystals themselves [37–40]. Additionally, a significant feature in the λ_e = 660 nm spectra is the broad band at 1580 to 1640 cm⁻¹. For carbonaceous samples, a band at 1580 cm⁻¹ is typically designated as the bond stretching mode in sp² carbon or the ‘G-band’. In this work, however, the band is closer towards 1620 cm⁻¹ and is designated the D’-band which in the absence of a 1350 cm⁻¹ disordered D-band typically refers to clusters of C=C bonded chains for sp³ rich and diamond like carbon materials [41]. This band is thus associated with significant concentrations of NDC impurities.

For the 3% sample, the NDC Band is much lower in intensity than the sp³ peak, implying fairly low NDC impurities. As the CH₄ concentration is increased to 5%, a considerable increase in NDC is found such that the intensity is much higher than the sp³ peak. Fig. 7f shows the peak intensity ratio of the NDC/sp³ contributions, clearly demonstrating the significant increase in NDC in 5A compared to the others. This is fairly well-known for diamond recipes with increased CH₄ concentration [32–34]. The recipe with O₂ in the gas phase (t ≈ 116 μm) appears to significantly reduce the NDC incorporation on the seeded side. The FWHM is generally a useful indicator of crystallite quality [42], which is much broader with the samples with O₂ at 2.2 to 2.6 cm⁻¹ as opposed to ~1.2 to 1.8 cm⁻¹ without. This suggests that although there is a lower NDC incorporation at the growth side, the polycrystalline structure consists of more sporadic grain sizes and therefore a higher density of grain boundaries.

Fig. 8 shows the multi-wavelength PL spectra. At all wavelength excitations, a broad PL background is measured which is typically found in PCD. Minimal evidence is found for the neutral nitrogen vacancy complex NV⁰ (~575 cm⁻¹) implying low nitrogen impurities [39]. This background appears to increase with higher CH₄ concentration as is shown for sample 5A. Additionally, a prominent feature is the peak associated with SiV centres (~738 nm) which becomes easier to identify with longer wavelengths. This is likely caused by plasma etching of the Si growth substrate and incorporation of these impurities into the diamond before the film coalesces. This is noticed for sample 3A and 5A, where in the case of the latter, this response dominates the spectra over the Raman line. For 4AO, the PL background is also similar to 3A, however, it is shown that the SiV peak is significantly reduced which suggests that O₂ in the gas phase suppresses the incorporation of Si.

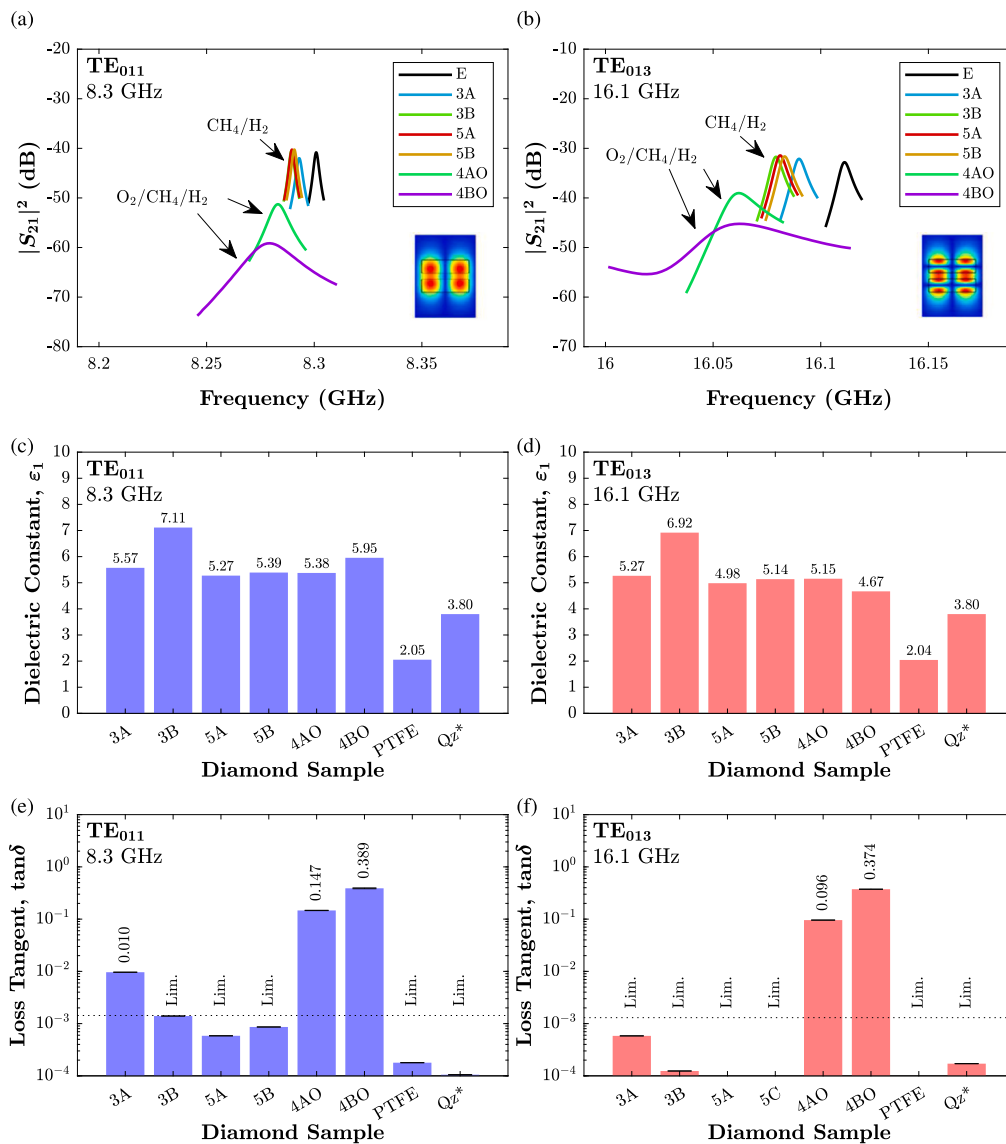


Fig. 6. MSDR measurements of diamond samples grown with different recipes. (a) and (b) show S_{21} traces of the TE_{011} and TE_{013} modes, respectively with FEM E-field shown in the inset. 'E' denotes unperturbed, '3', '4' and '5' denote the CH_4/H_2 percentage while 'O' denotes a 0.4% O_2/H_2 ratio. x scales are fixed to a 200 MHz span and y scales to 60 dB. (c) and (d) shows the dielectric constant and (e) and (f) loss tangent at 8.3 and 16.1 GHz, respectively, calibrated to a quartz standard denoted ** .

4.2. Diamond annealing

Fig. 9a and b shows the traces for the 3A sample incrementally annealed at 800 °C. It is clear that vacuum annealing for durations less than 7 h does not result in a significant change in microwave absorption. This suggest only a small fraction of the diamond crystals are being converted to NDC. Fig. 9c and d shows the calculated dielectric constant only marginally changes at 8.3 GHz and 16.1 GHz as is shown by the small shifts in frequency. Fig. 9e and f shows that at 15 h, however, the Q factor is noticeably lower, translating to an increased dielectric loss tangent from 0.01 and immeasurable to 0.06 and 0.04, at 8.3 GHz and 16.1 GHz, respectively. Note that even for a diamond sample with a significantly darker colour, as shown in Table 1, the dielectric loss is still lower than the samples grown with O_2 .

Fig. 10a to c shows the Raman spectra of 3A after each increment of vacuum annealing. At a laser excitation of $\lambda_e = 473$ and 532 nm, a similar spectra is obtained for all increments. Fig. 10d shows that for $\lambda_e = 473$ nm, the sp^3 diamond peak clearly reduces from 1333.6 cm^{-1} to 1332 cm^{-1} . However for $\lambda_e = 532$ and $\lambda_e = 660$ nm, the position

randomly shifts around 1332 cm^{-1} . While the former implies a relaxation of internal compressive stress in the film with annealing, higher wavelengths suggest random fluctuations in stress, again demonstrating the sensitivity of using UV lasers for stress measurements in the diamond crystals [38]. Fig. 10e there is minimal difference in FWHM as the film is annealed, implying no significant change in the crystallinity of the film during the annealing process besides a reduction in stress. Fig. 10f shows that as with the previous diamond set, the $\lambda_e = 660$ nm wavelength shows the NDC Band is clearly intensifying compared to the sp^3 peak when annealed, therefore implying that NDC impurities increase significantly at the seed side with incremental annealing time. Aside from this, the film at 15 h is also noticeably darker.

Fig. 11 shows the PL spectra of 3A at the start and end of cumulative vacuum annealing for 15 h. At all wavelength excitations, the same broad PL background is measured with the SiV band (~ 738 nm). After annealing, this SiV band becomes far more significant, likely owing to the reduction in the Raman line due to conversion of sp^3 into NDC as opposed to an increase in SiV centres. Besides this feature, there is minimal difference between the before and after spectra.

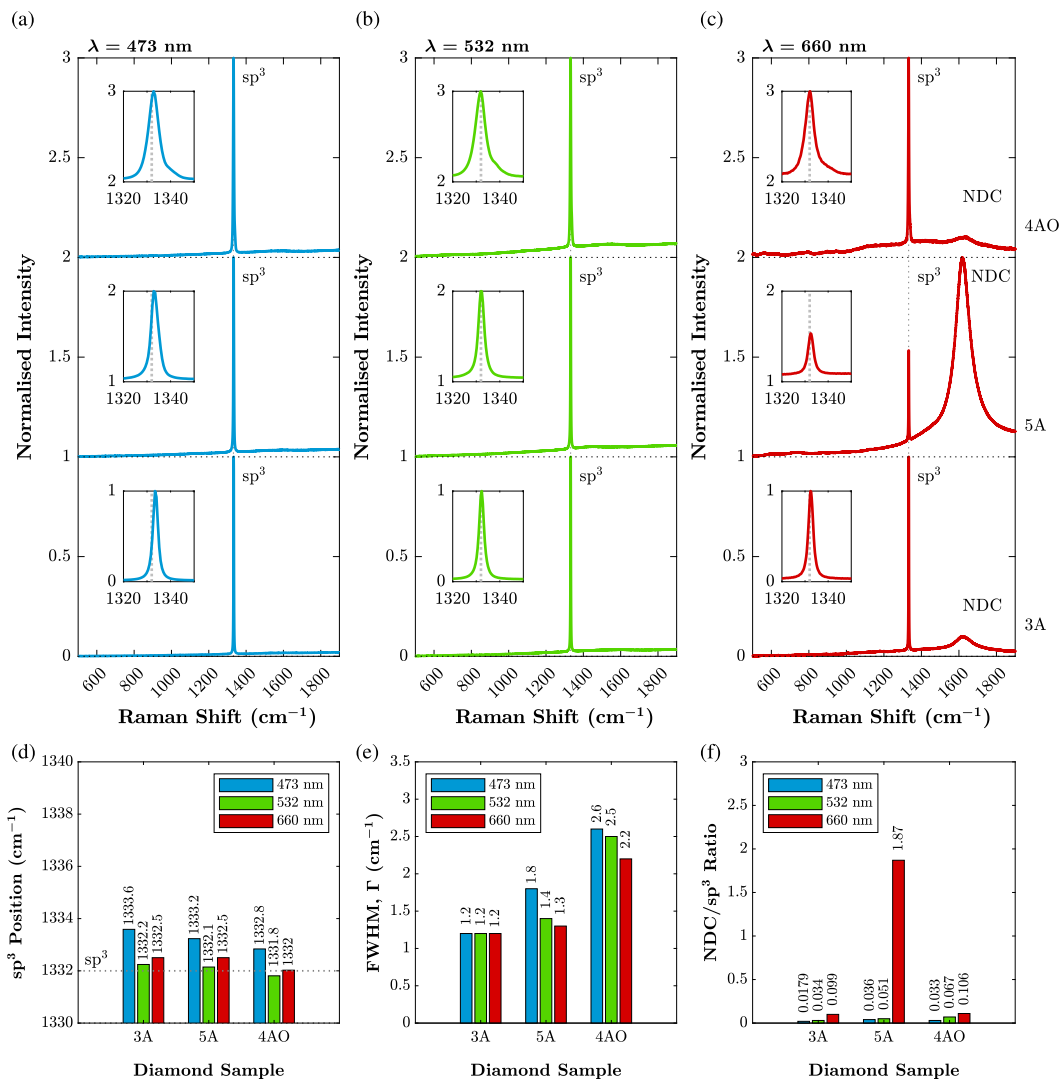


Fig. 7. Raman spectra ($\lambda_e = 473, 532$ and 660 nm) of diamond plates. (a), (b) and (c) shows diamond plates grown with different recipes (CH_4/H_2 at 3%, 5% and CH_4/H_2 at 4% and O_2/H_2 at 0.2%) at different wavelengths. All spectra are normalised to the maximum with a constant background removed and insets showing a magnified view of the diamond peak at ~ 1332 cm⁻¹. (b) and (c) show the Lorentzian fitted sp³ peak position and FWHM, respectively and (d) shows the peak intensity ratio of the NDC band to the sp³ peak.

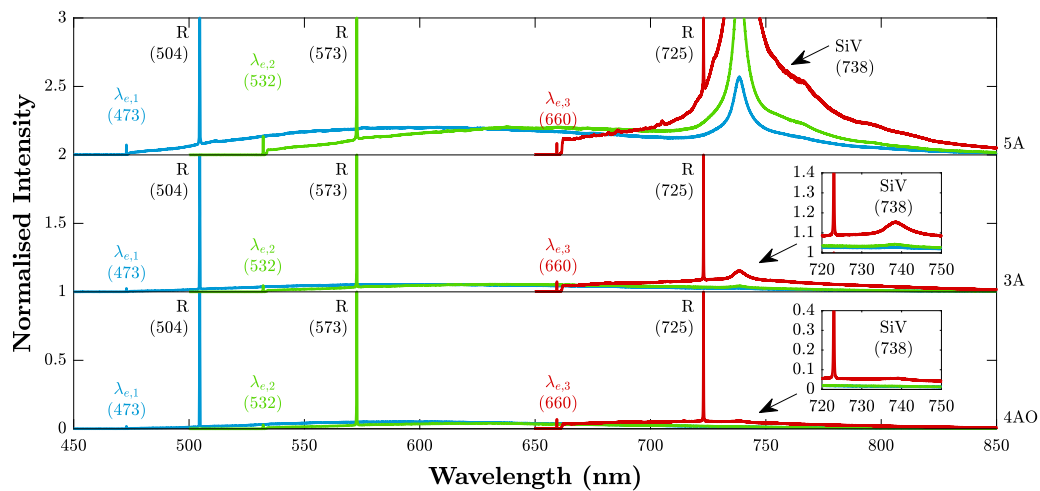


Fig. 8. PL spectra ($\lambda_e = 473, 532$ and 660 nm) of diamond plates grown with different recipes (CH_4/H_2 at 3%, 5% and CH_4/H_2 at 4% and O_2/H_2 at 0.2%). All spectra are normalised to the Raman line 'R' with insets showing magnified views of the SiV peak at 738 nm.

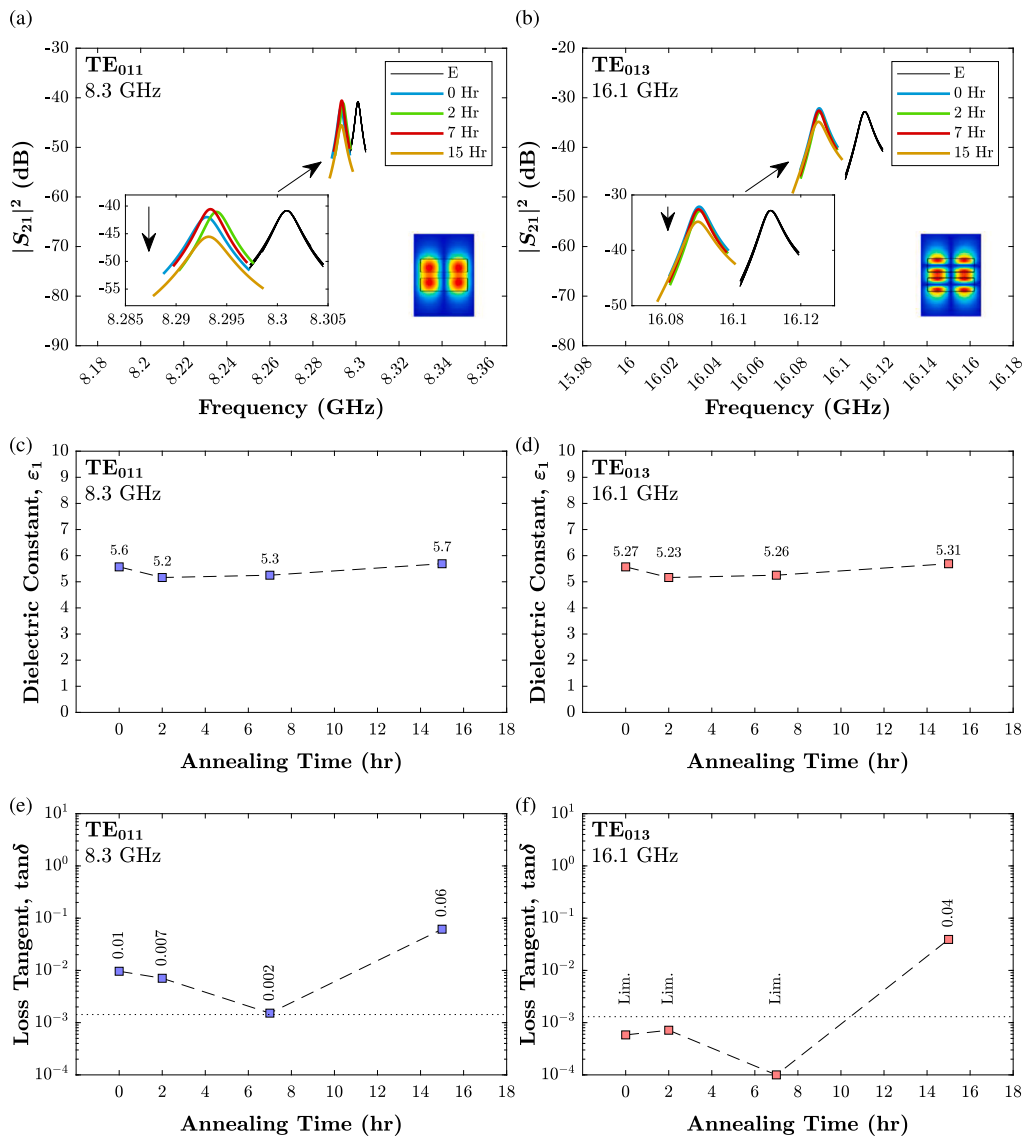


Fig. 9. MSDR measurements of the vacuum annealed 3A diamond sample. (a) and (b) show S_{21} traces of the TE₀₁₁ and TE₀₁₃ modes, respectively with FEM E-field shown in the inset. 'E' denotes the empty response, '0 Hr', '2 Hr', '7 Hr' and '15 Hr' denote the annealing duration at 800 °C. All x scales are fixed at 200 MHz and y scales to a 60 dB range. (c) and (d) show the calculated dielectric constant and (e) and (f) loss tangent, respectively.

4.3. SEM

Fig. 12 shows SEM images of the growth side of the PCD films used in this study. All images clearly show a coalesced film with large crystals and random grain morphologies. Samples 3B, 3A-15 and 5A both show similar grain structures, with sporadic surface impurities on both 3B and 5A. The grains in 5A are larger than 3B due to the increased film thickness. 3A-15 shows patches of rougher regions which is likely NDC carbon that is formed during the annealing process. The contrast from the brighter spots is likely charging caused by diamond that is not converted to NDC (as shown in the inset). 4AO shows the largest crystals owing to the thickness of the film, with some evidence of (111) triangular crystal growth. Interestingly, 4AO also shows the cleanest growth side of all of the films, despite being the most microwave lossy.

5. Discussion

This study suggests the controversial and less widely reported result that CVD diamond growth recipes with O₂ in the gas phase, while known for producing colourless and high 'quality' diamond, can also result in a significantly high microwave $\tan\delta_e$. The cause of this loss is

also less likely to be related to high concentrations of NDC impurities at the seed interface. The difference in the NDC band is significant between 3 and 5% CH₄/H₂, and yet there is little to no difference in the microwave complex permittivity. Only when large concentrations of NDC and sp² carbon are present in PCD films does the microwave $\tan\delta_e$ increase. Several studies on diamond particles corroborate this finding of increased absorption with increasing NDC and sp² carbon impurities [20,22,23,43]. However, it is particularly well-known that O₂ suppresses the formation of large concentrations of NDC impurities in H₂ [33,44,45], making this less likely to be the culprit for a large microwave $\tan\delta_e$. Thus, this discussion focuses on other ways O₂ grown samples could introduce a microwave absorbing effect.

Firstly, the dominant dielectric polarisation mechanisms in any material are those from electronic, ionic, dipole and interfacial polarisation. For diamond in the microwave frequency range, ionic and dipole polarisation can be discounted, leaving electronic polarisation (displacement of bound electrons around carbon atoms) and interfacial polarisation (free electrons which can migrate over percolating and short conduction pathways until they are met by a high energy barrier). Since electronic polarisation is very fast, this only contributes to ϵ'_r and the relaxation loss mechanics do not contribute to ϵ''_r at

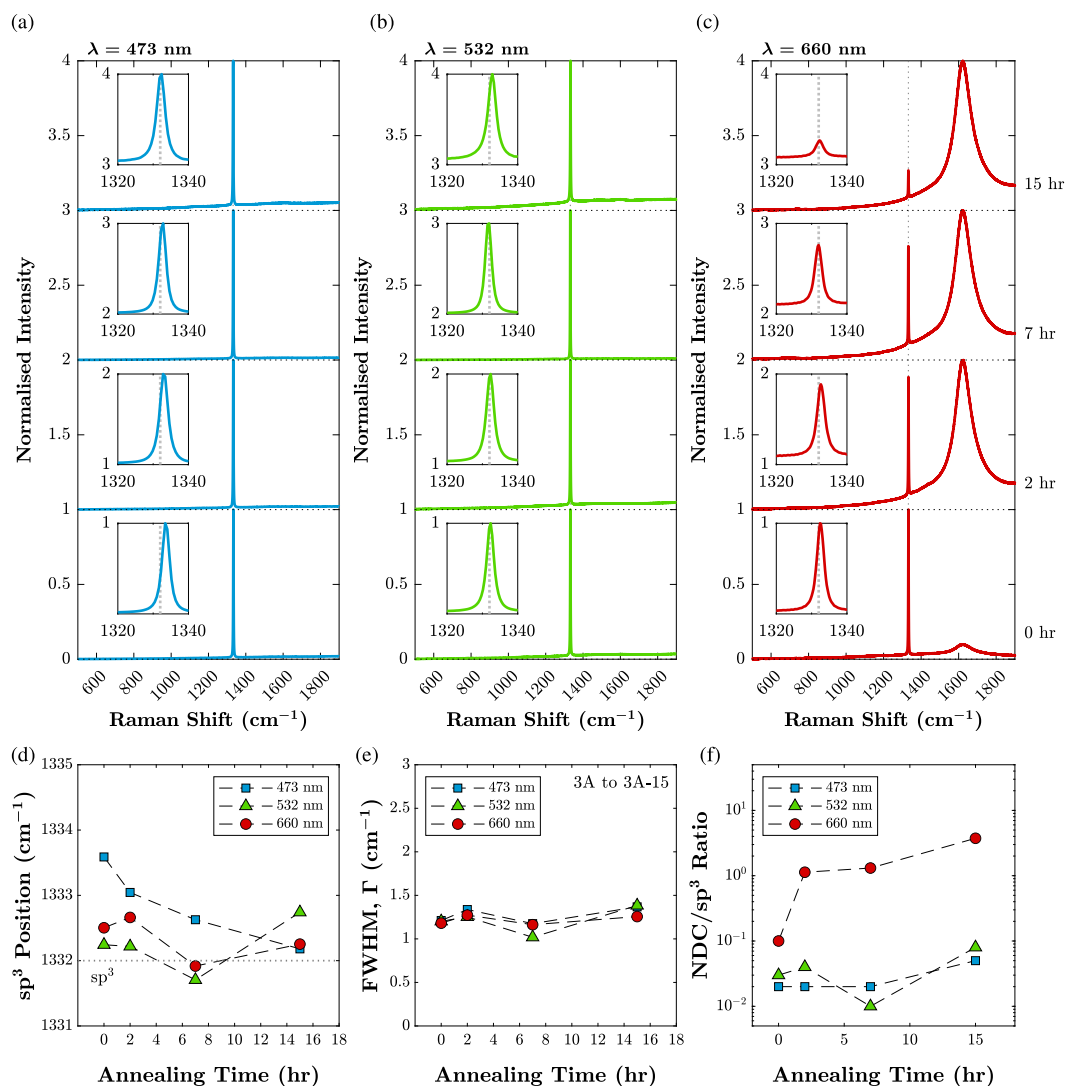


Fig. 10. Raman spectra ($\lambda = 473, 532$ and 660 nm) of the annealed diamond plate. (a), (b) and (c) show spectra of 3A grown at 3% CH_4/H_2 that has been subsequently annealed at 800°C for 2, 7 and 15 h at different wavelengths. All spectra are normalised to the maximum with a constant background removed and insets showing a magnified view of the diamond peak at $\sim 1332\text{ cm}^{-1}$. (b) and (c) show the Lorentzian fitted sp^3 peak position and FWHM, respectively.

gigahertz frequencies. In the case of PCD, the diamond grains act as the insulating barriers and grain boundaries or conducting impurities act as the transport pathways. Oxygen introduced during PCD growth must therefore introduce either conducting impurities or more grain boundaries in PCD.

The incorporation of electrically conducting impurities, however, seems implausible. The reduction of the Si-V emission implies that it is not related to Si. Additionally, previous studies with O_2 in the gas phase also show reduced Si-V centres [46]. N_2 is also not the likely reason owing to the low PL background in both Raman and PL data and the absence of a significant NV^0 peak. Although, there have been reports of high levels of O_2 in the gas phase, resulting in a higher N_2 impurity incorporation [42]. Direct hydrogen incorporation into the bulk film at the grain boundaries is likely not the reason since previous studies using Ar/CH_4 gas mixtures have shown that hydrogen termination at the grain boundaries is useful for low dielectric loss micro-crystalline diamond [47]. The surface conducting phenomenon of hydrogenated diamond is another potential reason [48], with surface conductivity being shown to be more stable with sub-surface incorporation from O_2/H_2 plasma treatment [49]. However, Tang et al. report that O_2 in the gas phase significantly reduces hydrogen incorporation, as identified by a reduction in the C-H stretching band in FTIR [50]; certainly a topic of

controversy. Finally, the cause is not likely due to the direct oxygenation or incorporation of O_2 into the PCD during growth since several experimental studies demonstrate that increased surface oxygenation of diamond significantly increases the sheet resistance [51]. DFT studies of oxygen-doped diamond also suggest it to be thermodynamically stable but with mid-gap impurity states that would not be measurable at room temperature [52]. Based on this literature, the origin of this increased microwave loss in O_2 grown PCD films is likely not due to O_2 incorporation, nor is it related to large concentrations of NDC, N_2 , Si and H_2 . Hence an impurity based origin for the microwave loss remains unaccounted.

The data presented here certainly points towards a grain boundary transport mechanism since the macroscopic crystalline quality is certainly worse, as inferred by the broad FWHM in the O_2 grown samples, despite the larger thickness. Previous work by Liu et al. show that films with a greater concentration of structural defects produced a larger Raman FWHM in addition to an increased microwave $\tan \delta_2$ [53]. Additionally, this may not necessarily result in any measurable D or G Band and highlights the importance of Raman sensitivity. Thus the broadening of the FWHM implies a higher concentration of grain boundaries whereby surface states, dangling bonds and very localised sp^2 bonding that are not detectable by Raman pertains to a contributor to electrical transport on un-terminated surfaces of diamond [54,55].

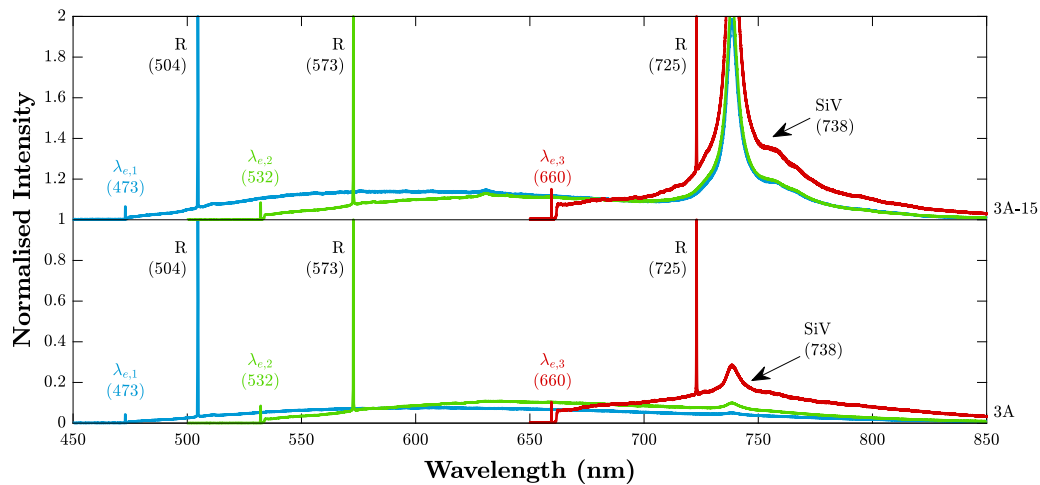


Fig. 11. PL spectra of vacuum annealed diamond plates: (bottom) initial film and (top) annealed film. All spectra are normalised to the Raman line 'R'.

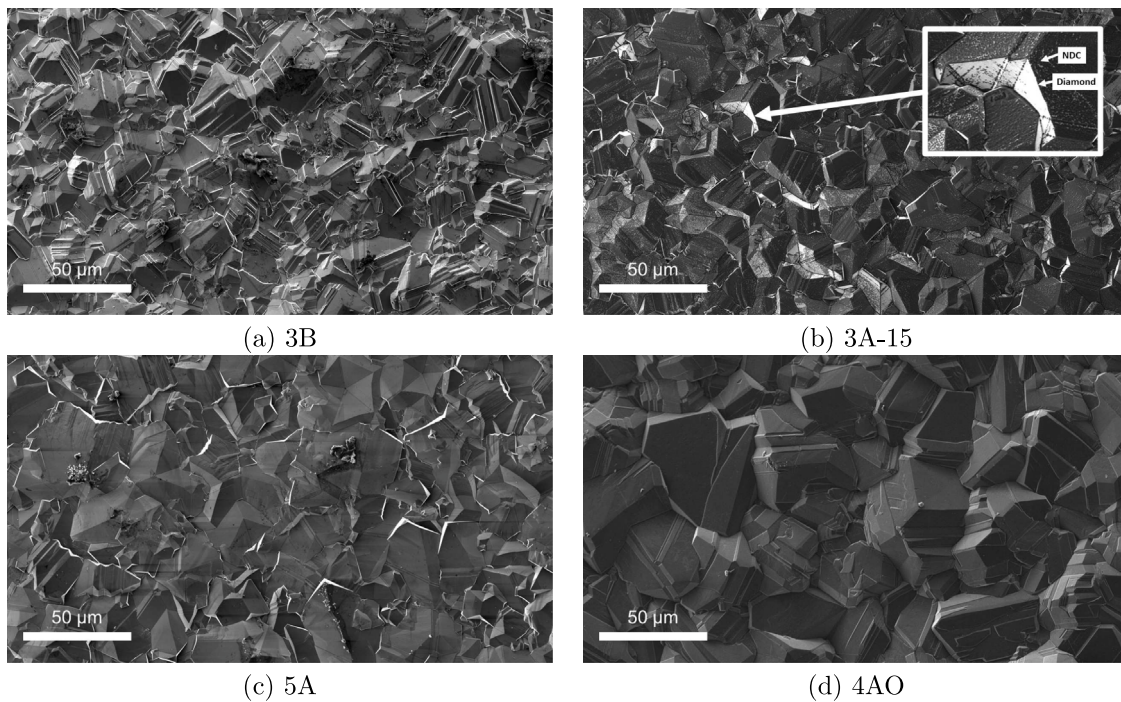


Fig. 12. SEM images of PCD diamond plates used in this study. Inset shows a magnified image of the annealed diamond plate, revealing clear contrasts in the smooth diamond region and rough NDC regions.

In PCD, Fiegl et al. have demonstrated that the frequency dependent electrical conductivity has been shown to be due to a single hopping transport mechanism due to the considerably high concentration of grain boundaries [56]. Thus, this work therefore points towards a grain boundary hopping transport mechanism that is not related to H or O termination.

Assuming the thermal conductivity remains sufficiently high in these oxygen grown PCD samples, this potentially opens avenues to another route to high thermal conductivity microwave attenuator films. High loss tangent microwave absorbers can be achieved with boron doping (concentration of $> 10^{20} \text{ cm}^{-3}$) [23,57,58] although, the caveat of using boron is that it severely contaminates the growth chamber.

Using oxygen based PCD recipes is a potentially more attractive solution to tuning the microwave properties of a diamond substrate. Additionally, in the utilisation of diamond substrates for increasing the quality factor of high kinetic inductance superconducting microwave diamond devices [59,60], this system is a valuable tool for screening diamond substrates before boron doped diamond is deposited.

6. Conclusion

This work presents an X-band microwave dielectric measurement system for PCD plates and demonstrates differences in diamonds grown with various recipes. Practically, the presented MSDR is an incredibly

simple and powerful technique as a dielectric quality control system for diamond dielectric substrates; the MCP VNA microwave trace alone demonstrates high and low quality microwave diamond dielectrics. However the greatest limitation is the loss tangent measurement limit which is determined by the ceramic dielectrics of the test fixture. While this study demonstrates the overall principle using commercially obtained dielectric resonators, the measurement sensitivity can be improved significantly using fused quartz, sapphire or even diamond (but at the expense of requiring larger area films for the same resonant frequency). This work also demonstrates that PCD grown with O₂ can result in very lossy microwave dielectrics, a result that is not so widely reported but can be investigated easily with microwave technique.

CRedit authorship contribution statement

Jerome A. Cuenca: Conceptualization, Data curation, Formal analysis, Investigation, Methodology, Software, Validation, Visualization, Writing – original draft. **Soumen Mandal:** Methodology. **Jaspa Stritt:** Methodology. **Xiang Zheng:** Methodology. **James Pomeroy:** Supervision, Writing – review & editing. **Martin Kuball:** Funding acquisition, Supervision, Resources. **Adrian Porch:** Conceptualization, Funding acquisition, Resources, Supervision, Writing – review & editing. **Oliver A. Williams:** Funding acquisition, Resources, Supervision, Writing – review & editing.

Declaration of competing interest

The authors declare that they have no known competing financial interests or personal relationships that could have appeared to influence the work reported in this paper.

Acknowledgements

This project has been supported by Engineering and Physical Sciences Research Council (EPSRC) under the “GaN-DaME” program grant (EP/P00945X/1) and the Innovate UK funded “CSconnected” Strength in Places Fund (107134). SEM was carried out in the clean-room of the ERDF-funded Institute for Compound Semiconductors (ICS) at Cardiff University with technical assistance from Thomas Peach and Michael Lewis. Special thanks is given to Andrew Rankmore from at Cardiff University for the workshop manufacturing. Data to support this publication can be found at: <http://dx.doi.org/10.17035/d.2024.0307934368>.

References

- [1] B. Fiegl, R. Kuhnert, H. Schwarzbauer, F. Koch, Diamond films as thermal conductors and electrical insulators applied to semiconductor power modules, *Diam. Relat. Mater.* 3 (4–6) (1994) 658–662, [http://dx.doi.org/10.1016/0925-9635\(94\)90244-5](http://dx.doi.org/10.1016/0925-9635(94)90244-5).
- [2] F. Faili, G. Williams, T. Obeloer, D.J. Twitchen, Diamond resistives - the passive way to manage the heat and keep the VSWR low at high frequencies, in: 2019 18th IEEE Intersoc. Conf. Therm. Thermomechanical Phenom. Electron. Syst. No. II, IEEE, 2019, pp. 137–140, <http://dx.doi.org/10.1109/ITHERM.2019.8757463>.
- [3] F.N. Faili, C. Engdahl, E. Francis, GaN-on-diamond substrates for HEMT applications, *Diam. Tool. J.* 1 (2009) 52–55.
- [4] J.G. Felbinger, M.V. Chandra, Y. Sun, L.F. Eastman, J. Wasserbauer, F. Faili, D. Babic, D. Francis, F. Ejeckam, Comparison of GaN HEMTs on diamond and SiC substrates, *IEEE Electron Device Lett.* 28 (11) (2007) 948–950, <http://dx.doi.org/10.1109/LED.2007.908490>.
- [5] J.J. Choi, Dielectric measurements of CVD diamonds at millimeter wavelength using a Fabry–Perot open resonator, *Int. J. Infrared Millim. Waves* 26 (10) (2005) 1427–1436, <http://dx.doi.org/10.1007/s10762-005-8440-5>.
- [6] H. Yamada, A. Meier, F. Mazzocchi, S. Schreck, T. Scherer, Dielectric properties of single crystalline diamond wafers with large area at microwave wavelengths, *Diam. Relat. Mater.* 58 (2015) 1–4, <http://dx.doi.org/10.1016/j.diamond.2015.05.004>.
- [7] V.I. Polyakov, A.I. Rukovichnikov, B.M. Garin, L.A. Avdeeva, R. Heidinger, V.V. Parshin, V.G. Ralchenko, Electrically active defects, conductivity, and millimeter wave dielectric loss in CVD diamonds, *Diam. Relat. Mater.* 14 (3–7) (2005) 604–607, <http://dx.doi.org/10.1016/j.diamond.2004.10.001>.

- [8] B.M. Garin, V.V. Parshin, V.I. Polyakov, A.I. Rukovichnikov, E.A. Serov, O.S. Mochevaeva, C.C. Jia, W.Z. Tang, F.X. Lu, Dielectric properties and applications of CVD diamonds in the millimeter and terahertz ranges, in: *Recent Adv. Broadband Dielectr. Spectrosc.*, IEEE, 2013, pp. 79–87.
- [9] M.Q. Ding, L. Li, J. Feng, Composite diamond films for short-mm wave and THz traveling wave tube windows, *Diam. Relat. Mater.* 50 (2014) 129–134, <http://dx.doi.org/10.1016/j.diamond.2014.09.009>.
- [10] A. Ibarra, M. González, R. Vila, J. Mollá, Wide frequency dielectric properties of CVD diamond, *Diam. Relat. Mater.* 6 (5–7) (1997) 856–859, [http://dx.doi.org/10.1016/S0925-9635\(96\)00724-8](http://dx.doi.org/10.1016/S0925-9635(96)00724-8).
- [11] Y. Liu, M. Ding, J. Su, Y. Li, P. Zhang, X. Lu, W. Tang, Dielectric properties of nitrogen-doped polycrystalline diamond films in Ka band, *Diam. Relat. Mater.* 76 (February) (2017) 68–73, <http://dx.doi.org/10.1016/j.diamond.2017.04.009>.
- [12] M. Janezic, E. Kuester, J. Jarvis, Broadband complex permittivity measurements of dielectric substrates using a split-cylinder resonator, in: 2004 IEEE MTT-S Int. Microw. Symp. Dig. (IEEE Cat. No.04CH37535), IEEE, 2004, pp. 1817–1820, <http://dx.doi.org/10.1109/MWSYM.2004.1338956>.
- [13] D. Munalli, G. Dimitrakis, D. Chronopoulos, S. Greedy, A. Long, Electromagnetic shielding effectiveness of carbon fibre reinforced composites, *Composites B* 173 (April) (2019) 106906, <http://dx.doi.org/10.1016/j.compositesb.2019.106906>.
- [14] F. Steinhagen, W. Haydl, T. Krens, W. Marsetz, R. Locher, C. Wild, P. Koidl, A. Hulsmann, T. Kerstenbrock, P. Heide, Microwave properties of coplanar transmission lines and filters on diamond from 1–120 GHz, in: *IEEE MTT-S*, Vol. 2, IEEE, 1998, pp. 1065–1068, <http://dx.doi.org/10.1109/MWSYM.1998.705177>.
- [15] V. Parshin, S. Myasnikova, V. Derkach, S. Tarapov, B. Garin, V. Polyakov, A. Rukovichnikov, R. Heidinger, I. Danilov, J. Molla, V. Ralchenko, Dielectric losses in CVD diamonds at frequencies 1 khz - 360 GHz and temperatures 0.9-900 K, in: *Int. Conf. Infrared Millim. Waves*, Vol. 1, No. 1, IEEE, 2005, pp. 22–23, <http://dx.doi.org/10.1109/ICIMW.2005.1572387>.
- [16] J. Molla, A. Ibarra, J. Margineda, J. Zamarró, A. Hernandez, Dielectric property measurement system at cryogenic temperature and microwave frequencies, *IEEE Trans. Instrum. Meas.* 42 (4) (1993) 817–821, <http://dx.doi.org/10.1109/19.234491>.
- [17] J.-M.L. Floch, R. Bara, J.G. Hartnett, M.E. Tobar, D. Mouneyrac, D. Passerieux, D. Cros, J. Krupka, P. Goy, S. Carroopen, Electromagnetic properties of polycrystalline diamond from 35 K to room temperature and microwave to terahertz frequencies, *J. Appl. Phys.* 109 (9) (2011) 094103, <http://dx.doi.org/10.1063/1.3580903>.
- [18] J. Krupka, K. Derzakowski, B. Riddle, J. Baker-Jarvis, A dielectric resonator for measurements of complex permittivity of low loss dielectric materials as a function of temperature, *Meas. Sci. Technol.* 9 (1999) 1751–1756, <http://dx.doi.org/10.1088/0957-0233/9/10/015>.
- [19] J. Krupka, S.A. Gabelich, K. Derzakowski, B.M. Pierce, Comparison of split post dielectric resonator and ferrite disc resonator techniques for microwave permittivity measurements of polycrystalline yttrium iron garnet, *Meas. Sci. Technol.* 10 (11) (1999) 1004–1008, <http://dx.doi.org/10.1088/0957-0233/10/11/305>.
- [20] D. Slocombe, A. Porch, E. Bustarret, O.A. Williams, Microwave properties of nanodiamond particles, *Appl. Phys. Lett.* 102 (24) (2013) 244102, <http://dx.doi.org/10.1063/1.4809823>.
- [21] A. Porch, D.I. Odili, P.A. Childs, Microwave characterisation of carbon nanotube powders, *Nanoscale Res. Lett.* 7 (429) (2012) 1–5, <http://dx.doi.org/10.1186/1556-276X-7-429>.
- [22] J.A. Cuenca, K.J. Sankaran, P. Pobedinskas, K. Panda, I.-N. Lin, A. Porch, K. Haenen, O.A. Williams, Microwave cavity perturbation of nitrogen doped nanocrystalline diamond films, *Carbon* 145 (2019) 740–750, <http://dx.doi.org/10.1016/j.carbon.2018.12.025>.
- [23] J.A. Cuenca, S. Sugai, S. Nakamura, Y. Miyake, D.J. Morgan, T. Kondo, E.L. Thomas, S. Mandal, A. Porch, O.A. Williams, Microwave conductivity of boron-doped nanodiamond particles, *APMC*, 2022, pp. 145–147, <http://dx.doi.org/10.23919/apmc55665.2022.9999762>.
- [24] D.M. Pozar, *Microwave Engineering*, fourth ed., Wiley, 2011.
- [25] O.A. Williams, O. Douhéret, M. Daenen, K. Haenen, E. Osawa, M. Takahashi, Enhanced diamond nucleation on monodispersed nanocrystalline diamond, *Chem. Phys. Lett.* 445 (4–6) (2007) 255–258, <http://dx.doi.org/10.1016/j.cplett.2007.07.091>.
- [26] S. Mandal, Nucleation of diamond films on heterogeneous substrates: a review, *RSC Adv.* 11 (17) (2021) 10159–10182, <http://dx.doi.org/10.1039/d1ra00397f>.
- [27] J.A. Cuenca, S. Mandal, E.L. Thomas, O.A. Williams, Microwave plasma modelling in clamshell chemical vapour deposition diamond reactors, *Diam. Relat. Mater.* 124 (November 2021) (2022) 108917, <http://dx.doi.org/10.1016/j.diamond.2022.108917>, [arXiv:2111.10258](https://arxiv.org/abs/2111.10258).
- [28] J.A. Cuenca, M.D. Smith, D.E. Field, F. C.P. Massabuau, S. Mandal, J. Pomeroy, D.J. Wallis, R.A. Oliver, I. Thayne, M. Kuball, O.A. Williams, Thermal stress modelling of diamond on GaN/III-Nitride membranes, *Carbon* 174 (2021) 647–661, <http://dx.doi.org/10.1016/j.carbon.2020.11.067>.
- [29] M.D. Smith, J.A. Cuenca, D.E. Field, Y.-c. Fu, C. Yuan, F. Massabuau, S. Mandal, J.W. Pomeroy, R.A. Oliver, M.J. Uren, K. Elgaid, O.A. Williams, I. Thayne, M. Kuball, GaN-on-diamond technology platform: Bonding-free membrane manufacturing process, *AIP Adv.* 10 (3) (2020) 035306, <http://dx.doi.org/10.1063/1.5129229>.

- [30] S. Mandal, C. Yuan, F. Massabuau, J.W. Pomeroy, J. Cuenca, H. Bland, E. Thomas, D. Wallis, T. Batten, D. Morgan, R. Oliver, M. Kuball, O.A. Williams, Thick, adherent diamond films on AlN with low thermal barrier resistance, *ACS Appl. Mater. Interfaces* 11 (43) (2019) 40826–40834, <http://dx.doi.org/10.1021/acsmi.9b13869>, arXiv:1907.02481.
- [31] M. Aslam, Bulk etching of silicon wafer and development of a polyimide membrane, *J. Phys. Conf. Ser.* 439 (1) (2013) 012029, <http://dx.doi.org/10.1088/1742-6596/439/1/012029>.
- [32] H. Windschmann, G.F. Epps, Free-standing diamond membranes: optical, morphological and mechanical properties, *Diam. Relat. Mater.* 1 (5–6) (1992) 656–664, [http://dx.doi.org/10.1016/0925-9635\(92\)90185-Q](http://dx.doi.org/10.1016/0925-9635(92)90185-Q).
- [33] T. Kawato, K.I. Kondo, Effects of oxygen on CVD diamond synthesis, *Japan. J. Appl. Phys.* 26 (9R) (1987) 1429–1432, <http://dx.doi.org/10.1143/JJAP.26.1429>.
- [34] A.P. Bolshakov, V.G. Ralchenko, V.Y. Yurov, A.F. Popovich, I.A. Antonova, A.A. Khomich, E.E. Ashkinazi, S.G. Ryzhkov, A.V. Vlasov, A.V. Khomich, High-rate growth of single crystal diamond in microwave plasma in CH₄/H₂ and CH₄/H₂/Ar gas mixtures in presence of intensive soot formation, *Diam. Relat. Mater.* 62 (2016) 49–57, <http://dx.doi.org/10.1016/j.diamond.2015.12.001>.
- [35] N.G. Ferreira, E. Abramof, N.F. Leite, E.J. Corat, V.J. Trava-Airoldi, Analysis of residual stress in diamond films by X-ray diffraction and micro-Raman spectroscopy, *J. Appl. Phys.* 91 (4) (2002) 2466–2472, <http://dx.doi.org/10.1063/1.1431431>.
- [36] J. Robertson, Diamond-like amorphous carbon, *Mater. Sci. Eng. R Rep.* 37 (4–6) (2002) 129–281, [http://dx.doi.org/10.1016/S0927-796X\(02\)00005-0](http://dx.doi.org/10.1016/S0927-796X(02)00005-0), arXiv:arXiv:1011.1669v3.
- [37] J. Wagner, C. Wild, P. Koidl, Resonance effects in Raman scattering from polycrystalline diamond films, *Appl. Phys. Lett.* 59 (7) (1991) 779–781, <http://dx.doi.org/10.1063/1.105340>.
- [38] Z. Sun, J. Shi, B. Tay, S. Lau, UV Raman characteristics of nanocrystalline diamond films with different grain size, *Diam. Relat. Mater.* 9 (12) (2000) 1979–1983, [http://dx.doi.org/10.1016/S0925-9635\(00\)00349-6](http://dx.doi.org/10.1016/S0925-9635(00)00349-6).
- [39] S. Praver, R.J. Nemanich, Raman spectroscopy of diamond and doped diamond, *Philos. Trans. R. Soc. London. Ser. A Math. Phys. Eng. Sci.* 362 (1824) (2004) 2537–2565, <http://dx.doi.org/10.1098/rsta.2004.1451>.
- [40] K.J. Sankaran, D.Q. Hoang, S. Kunuku, S. Korneychuk, S. Turner, P. Pobedinskas, S. Drijkoningen, M.K. Van Bael, J. D'Haen, J. Verbeeck, K.C. Leou, I.N. Lin, K. Haenen, Enhanced optoelectronic performances of vertically aligned hexagonal boron nitride nanowalls-nanocrystalline diamond heterostructures, *Sci. Rep.* 6 (March) (2016) 1–11, <http://dx.doi.org/10.1038/srep29444>.
- [41] M. Mermoux, S. Chang, H.A. Girard, J.C. Arnault, Raman spectroscopy study of detonation nanodiamond, *Diam. Relat. Mater.* 87 (May) (2018) 248–260, <http://dx.doi.org/10.1016/j.diamond.2018.06.001>.
- [42] T. Shimaoka, H. Yamada, Y. Mokuno, A. Chayahara, Oxygen concentration dependence in microwave plasma-enhanced chemical vapor deposition diamond growth in the (H, C, O, N) system, *Phys. Status Solidi Appl. Mater. Sci.* 219 (11) (2022) 1–8, <http://dx.doi.org/10.1002/pssa.202100887>.
- [43] J.A. Cuenca, E.L.H. Thomas, S. Mandal, D.J. Morgan, F. Lloret, D. Araujo, O.A. Williams, A. Porch, Microwave permittivity of trace sp² carbon impurities in sub-micron diamond powders, *ACS Omega* 3 (2) (2020) 2183–2192, <http://dx.doi.org/10.1021/acsomega.7b02000>, arXiv:abs/1906.06286.
- [44] C.F. Chen, Y.C. Huang, S. Hosomi, I. Yoshida, Effect of oxygen addition on microwave plasma CVD of diamond from CH₄-H₂ mixture, *Mater. Res. Bull.* 24 (1) (1989) 87–94, [http://dx.doi.org/10.1016/0025-5408\(89\)90013-5](http://dx.doi.org/10.1016/0025-5408(89)90013-5).
- [45] S.J. Harris, A.M. Weiner, Effects of oxygen on diamond growth, *Appl. Phys. Lett.* 55 (21) (1989) 2179–2181, <http://dx.doi.org/10.1063/1.102350>.
- [46] Y.N. Palyanov, G. Sakr, J. Barjon, Diamond & related materials high quality thick CVD diamond films homoepitaxially grown on (111)-oriented substrates, *Diam. Relat. Mater.* 41 (2014) 34–40, <http://dx.doi.org/10.1016/j.diamond.2013.11.002>.
- [47] C. Liu, X. Xiao, J. Wang, B. Shi, V.P. Adiga, R.W. Carpick, J.A. Carlisle, O. Auciello, Dielectric properties of hydrogen-incorporated chemical vapor deposited diamond thin films, *J. Appl. Phys.* 102 (7) (2007) 074115, <http://dx.doi.org/10.1063/1.2785874>.
- [48] O.A. Williams, R.B. Jackman, Surface conductivity on hydrogen terminated diamond, *Semicond. Sci. Technol.* 18 (3) (2003) S34–S40, <http://dx.doi.org/10.1088/0268-1242/18/3/305>.
- [49] W. Deferme, G. Tanasa, J. Amir, K. Haenen, M. Nešládek, C.F. Flipse, The role of (sub)-surface oxygen on the surface electronic structure of hydrogen terminated (100) CVD diamond, *Diam. Relat. Mater.* 15 (4–8) (2006) 687–691, <http://dx.doi.org/10.1016/j.diamond.2005.12.016>.
- [50] C. Tang, A. Neves, A. Fernandes, Study the effect of O₂ addition on hydrogen incorporation in CVD diamond, *Diam. Relat. Mater.* 13 (1) (2004) 203–208, <http://dx.doi.org/10.1016/j.diamond.2003.10.032>.
- [51] J. Navas, D. Araujo, J.C. Piñero, A. Sánchez-Coronilla, E. Blanco, P. Villar, R. Alcántara, J. Montserrat, M. Florentin, D. Eon, J. Pernot, Oxygen termination of homoepitaxial diamond surface by ozone and chemical methods: An experimental and theoretical perspective, *Appl. Surf. Sci.* 433 (2018) 408–418, <http://dx.doi.org/10.1016/j.apsusc.2017.10.065>.
- [52] M. Ullah, E. Ahmed, F. Hussain, A.M. Rana, R. Raza, H. Ullah, Electronic structure calculations of oxygen-doped diamond using DFT technique, *Microelectron. Eng.* 146 (2015) 26–31, <http://dx.doi.org/10.1016/j.mee.2015.02.040>.
- [53] Y.Q. Liu, M.H. Ding, J.J. Su, H. Ren, X.R. Lu, W.Z. Tang, An investigation on dielectric properties of diamond films in the range of K and Ka band, *Diam. Relat. Mater.* 73 (2017) 114–120, <http://dx.doi.org/10.1016/j.diamond.2016.08.007>.
- [54] P. Keblinski, S. Phillpot, D. Wolf, H. Gleiter, On the nature of grain boundaries in nanocrystalline diamond, *Nanostruct. Mater.* 12 (1–4) (1999) 339–344, [http://dx.doi.org/10.1016/S0965-9773\(99\)00130-0](http://dx.doi.org/10.1016/S0965-9773(99)00130-0).
- [55] F. Liu, Y. Cui, M. Qu, J. Di, Effects of hydrogen atoms on surface conductivity of diamond film, *AIP Adv.* 5 (4) (2015) <http://dx.doi.org/10.1063/1.4904057>.
- [56] B. Fiegl, R. Kuhnert, M. Ben-Chorin, F. Koch, Evidence for grain boundary hopping transport in polycrystalline diamond films, *Appl. Phys. Lett.* 65 (3) (1994) 371–373, <http://dx.doi.org/10.1063/1.112379>.
- [57] W. Gajewski, P. Achatz, O.A. Williams, K. Haenen, E. Bustarret, M. Stutzmann, J.A. Garrido, Electronic and optical properties of boron-doped nanocrystalline diamond films, *Phys. Rev. B* 79 (4) (2009) 1–14, <http://dx.doi.org/10.1103/PhysRevB.79.045206>.
- [58] M. Ding, Y. Liu, X. Lu, Y. Li, W. Tang, Boron doped diamond films: A microwave attenuation material with high thermal conductivity, *Appl. Phys. Lett.* 114 (16) (2019) 162901, <http://dx.doi.org/10.1063/1.5083079>.
- [59] J.A. Cuenca, T. Brien, S. Mandal, S. Manifold, S. Doyle, A. Porch, G.M. Klemencic, O.A. Williams, Superconducting boron doped nanocrystalline diamond microwave coplanar resonator, *Carbon* 201 (2023) 251–259, <http://dx.doi.org/10.1016/j.carbon.2022.08.084>, arXiv:2111.10258.
- [60] B. Oripov, D. Kumar, C. Garcia, P. Hemmer, T. Venkatesan, M.S. Ramachandra Rao, S.M. Anlage, Large microwave inductance of granular boron-doped diamond superconducting films, *Appl. Phys. Lett.* 118 (24) (2021) 242601, <http://dx.doi.org/10.1063/5.0051227>, arXiv:2103.14738.